Batteries & Supercaps

Research Article
doi.org/10.1002/batt.202400140

Chemistry Europe
European Chemical Societies Publishing

www.batteries-supercaps.org

Effect of Protic and Aprotic Formamide-Based Organic Electrolytes for Rechargeable Zinc/MnO_2 Battery

Abhishek Lahiri,*[a] Pranay Hirani,[a] and Sophia Haghani[b]

Zinc ion batteries (ZIBs) are emerging as a promising and cost-effective alternative energy storage system compared to other metal-ion batteries. Aqueous electrolytes have been extensively studied in Zn-ion batteries which has shown issues related to cathode dissolution. In comparison, little has been looked into the use of organic electrolytes in ZIBs. Here, we have studied both protic and aprotic forms of formamide-based organic electrolytes containing Zn trifluoromethanesulfonate and their influence on the Zn solvation chemistry, electrochemistry, and performance of Zn-MnO_2 battery. It was observed that protic-based electrolytes gave a much better capacity and stability for the Zn-MnO_2 battery. A capacity close to 150 mAh g^{-1} was obtained with formamide electrolyte at a current density of 0.25 A g^{-1}. For all the other formamide-based electrolytes tested, the capacity was lower. After 100 cycles, an average capacity retention of 72% was obtained for formamide-based electrolyte. This study shows that protic-based electrolytes might be a suitable option for non-aqueous-based Zn-ion batteries.

Introduction

The demand for portable electronic devices, transportation, and grid-storage applications is ever increasing, and therefore the need for efficient and economical storage devices having high power and energy density is needed.[1,2] Li-ion batteries (LIBs) have dominated the electronic markets in the last two decades and are now being used in the automobile sector. However, the main issue with LIBs is the limited availability of lithium along with difficulty in recycling the batteries.[3–5] Therefore, recently lot more effort has been focused on developing alternate battery chemistry based on earth-abundant and easily recyclable materials such as Na, Zn, Ca, and Al.[6–8]

Among the various battery chemistry, Zn-based batteries are attractive due to their low-cost, high theoretical capacity (820 mAh g^{-1}), safety of Zn metal, stability in aqueous electrolytes, and ease of recyclability.[9–11] Recently, ZIBs have received much attention as it was shown to intercalate and deintercalated into different host materials, such as vanadium oxide (V_2O_5) and manganese dioxide (MnO_2), as these metal oxides have a tunnel structure.[12–16] With MnO_2 cathodes, a capacity of 300 mAh g^{-1} was achieved based on co-intercalation of H^+ and Zn^{2+} ions.[14,15] However, it was observed that in aqueous electrolyte, MnO_2 dissolves with time and therefore Mn salts had to be added to maintain the capacity as further MnO_2 deposition takes place during the battery cycling.[14] Furthermore, in aqueous-based ZIBs, other issues also must be addressed such as Zn corrosion reaction at the anode, hydrogen evolution reaction during cycling, and loss of capacity due to side reactions that occur due to local changes in the pH of the electrolyte.[9,17] In order to reduce Zn corrosion and hydrogen evolution reaction, coatings on Zn have been shown to improve the cyclability.[18,19] However, issues would still remain if the defects occur in the coating with time.

In comparison to aqueous electrolytes, non-aqueous electrolytes such as organic solvents, deep eutectic solvents or ionic liquids can play a crucial role in improving the performance and stability of ZIBs.[20–22] Ionic liquids have been shown to inhibit Zn dendrite formation either by modulating the cationic or anionic Zn complex or by modifying the interface using an additive in the electrolyte.[22,23] However, the issue with ionic liquids is the high viscosity and low ionic conductivity. However, as ionic liquids modify the electrode/electrolyte interface which changes the nucleation/growth of Zn, lowering viscosity and improvement in diffusion kinetics is possible using ionic liquid-water electrolytes.[24] More recently, bio-ionic liquid-based electrolytes have shown to inhibit Zn dendrite formation which opens up new avenues in developing sustainable electrolytes.[25] Besides ionic liquids, polar aprotic solvents have also been investigated which avoid hydrogen evolution reaction reactions. Acetonitrile (AN) as a polar solvent has been studied with various Zn salts of Zn perchlorate ($Zn(ClO_4)_2$), Zn trifluoromethanesulfonate ($Zn(OTf)_2$), and Zn bis(trifluoromethylsulfonyl)imide ($Zn(TFSI)_2$) on different cathode materials which has shown reasonable capacity of about 120 mAh g^{-1}.[17,26,27] Recently, a higher dielectric aprotic solvent of dimethyl sulfoxide electrolyte containing $Zn(OTf)_2$ showed reasonable capacity of 159 mAh g^{-1} at 50 mA g^{-1} which decreased by 60% after 1000 cycles.[28] Despite their advantages, aprotic organic electrolytes do have a few issues, such large overpotential of Zn

[a] Dr. A. Lahiri, Mr. P. Hirani
Department of Chemical Engineering, Brunel University London, UB8 3PH Uxbridge, UK
E-mail: abhishek.lahiri@brunel.ac.uk

[b] Dr. S. Haghani
Experimental Techniques Centre, College of Engineering, Design and Physical Science, Brunel University London, Kingston Lane, UB8 3PH London, UK

Research Article
doi.org/10.1002/batt.202400140
Chemistry Europe
European Chemical Societies Publishing

deposition due to Zn complexation which affects the rate capability. Also, little is understood regarding the solvation/desolvation process.[11,21]

In this paper, we have studied a highly dielectric protic electrolyte of formamide (dielectric constant of 109[29]) containing $Zn(OTf)_2$ for a Zn-MnO_2 battery. We have studied the Zn solvation chemistry using Raman and infrared spectroscopy, Zn deposition/stripping process in a symmetric cell, and Zn electrochemistry on MnO_2 cathode. We have also studied the effect of the side chain of formamide with different dielectric constants (N methyl formamide, dielectric constant 186,[30] N, N dimethyl formamide, Dielectric constant 37[29] and N, N Diethyl formamide, dielectric constant[29]) on Zn electrochemistry and Zn-MnO_2 battery performance. Using different characterisation techniques, the studies revealed that the dielectric constant of the electrolyte plays an important role in the performance of the Zn battery.

Experimental

Sodium acetate (99.99%), Zn triflate (98%), $MnSO_4$ (98%), Formamide (99%), N-methyl formamide (NMF, 99%), dimethyl formamide (DMF, 99%), diethyl formamide (DEF, 99%) were purchased from Fisher Scientific. Zn (99.9%) was purchased from Pi-Kem and graphite paper was purchased from RS Pro. The electrolytes were prepared by mixing Zn triflate in different organic solvents at 70 °C for two hours after which it was cooled to room temperature before usage.

MnO_2 was electrochemically deposited onto the graphite paper from a solution of 0.2 M Na_2SO_4 containing 5 mM $MnSO_4$. The deposition was performed by cycling between a potential of 0 V to 1.5 V vs Ag/AgCl. Ten cyclic voltammetry cycles were performed to obtain MnO_2 on the graphite paper. The deposit was then washed in water and dried in a vacuum oven at 60 °C for two hours. The mass loading was found to be between 1–1.5 mg cm^{-2}. X-ray diffraction analysis confirmed that the electrodeposited MnO_2 was amorphous.

Electrochemical measurements were carried out in a home-built Teflon cell consisting of MnO_2 MnO2-coated graphite electrode as the working electrode, Zn foil as the counter, and reference electrodes with different electrolytes. CV was performed in the potential range of 0.5–2.2 V vs Zn at different scan rates from 1 to 5 mV s^{-1} by using a Biologic VMP 3e potentiostat/galvanostat. The galvanostatic charge/discharge cycling tests were carried out in a split cell with Zn anode, a Whatman separator, MnO_2 cathode with different electrolytes by using a battery tester Nanocycler from Nanobase.

The FTIR and Raman spectra of the electrolyte were acquired using Shimadzu IRspirit and Renishaw inVia confocal Raman microscope, equipped with a 514 nm laser (Stellar-REN) and using a diffraction grating of 1800 lines/mm with a Renishaw CCD camera as the detector, respectively. For Raman, the samples were run with laser power at 100% using the 5x objective lens with a 532 nm laser, respectively.

Results and Discussion

The Zn solvation in the electrolyte was studied using Fourier transform infrared spectroscopy (FTIR) and Raman spectroscopy. Figure 1a compares the IR spectra of $Zn(OTf)_2$ in different formamide-based protic and aprotic solvents. It is evident that there are changes in vibration modes in SO_3, CH, and NH_2 due to the interaction between the $Zn(OTf)_2$ and different formamide solvents. Compared to formamide, additional peaks due to the presence of side chains appear in the IR spectra in NMF, DMF and DEF.

Figure 1b compares the Raman spectra of the different electrolytes from which it is evident that changes are observed in vibration modes of formamide as well as CF_3 in the $Zn(OTf)_2$. Additional peaks such as ν_{HNH} at 1080 cm^{-1} are seen for DMF and DEF. It is well known that the vibration modes of the anions are sensitive to the changes in its surroundings from which metal ion solvation can be evaluated using Raman spectroscopy.[23,24,31] For the case of triflate anion, both theoretical and experimental studies revealed that the changes in CF_3 which occurs between 700 and 800 wavenumbers in the Raman spectra can be used to understand the metal ion

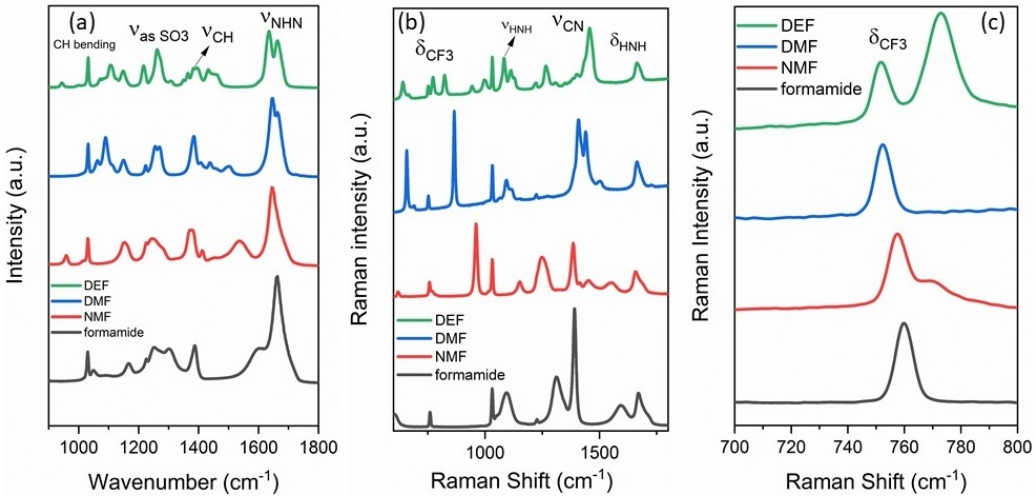

Figure 1. FTIR and Raman Spectra of different electrolytes, (a) IR spectra; (b) Raman spectra; and (c) magnified CF_3 peak of the Raman spectra.

Research Article
doi.org/10.1002/batt.202400140
Chemistry Europe
European Chemical Societies Publishing

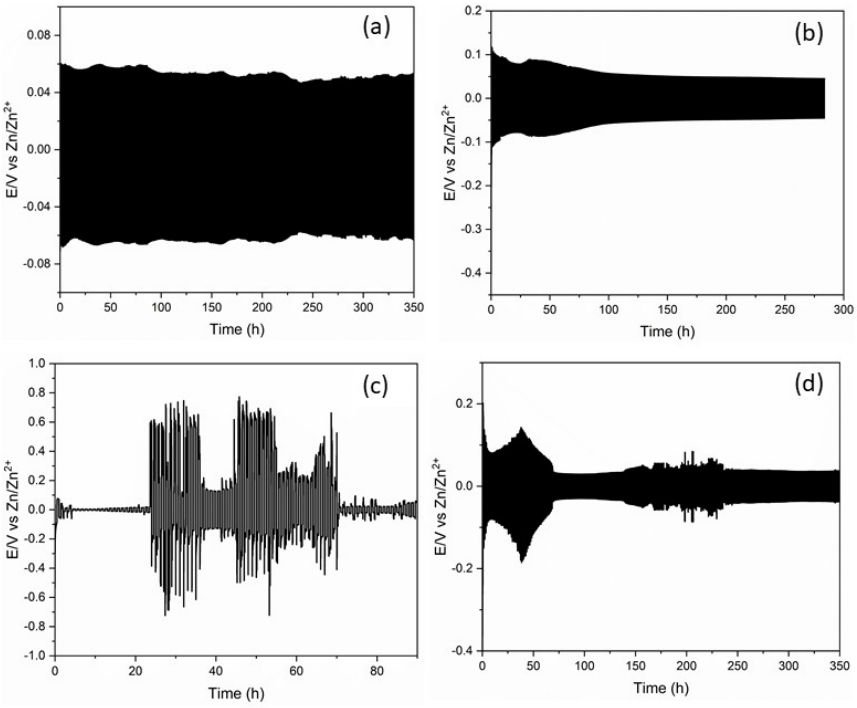

Figure 2. Zn deposition/stripping in a Zn/Zn symmetric cell at a current density of 1 mA cm^{-2} (capacity of 0.5 mAh cm^{-2}) in (a) 0.5 M $Zn(OTf)_2$ in formamide (b) 0.5 M $Zn(OTf)_2$ in NMF (c) 0.5 M $Zn(OTf)_2$ in DMF (d) 0.5 M $Zn(OTf)_2$ in DEF.

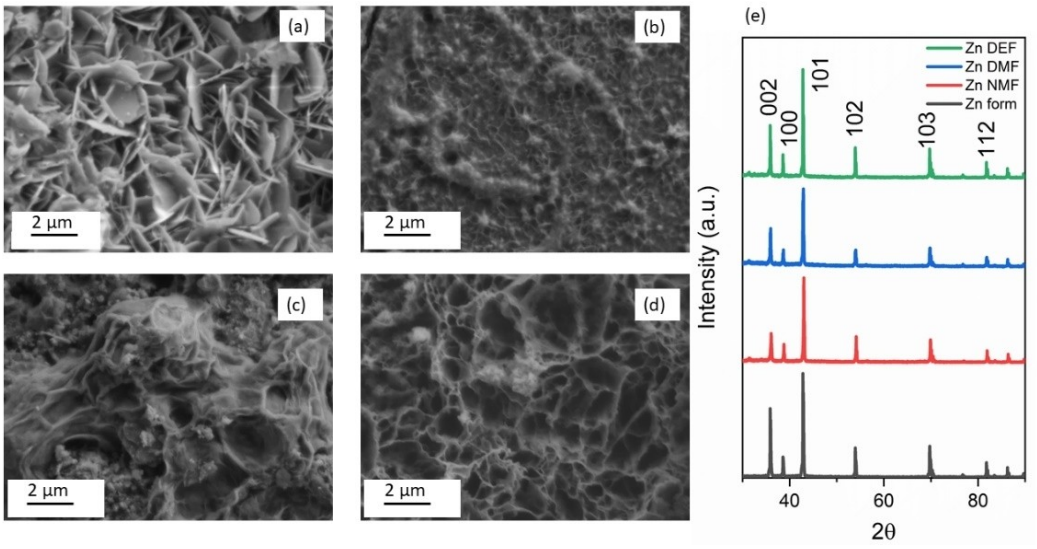

Figure 3. SEM of Zn after cycling at a current density of 1 mA cm^{-2} (capacity of 0.5 mAh cm^{-2}) in (a) 0.5 M $Zn(OTf)_2$ in formamide (b) 0.5 M $Zn(OTf)_2$ in NMF (c) 0.5 M $Zn(OTf)_2$ in DMF (d) 0.5 M $Zn(OTf)_2$ in DEF (e) XRD of Zn after cycling in different electrolytes.

complexation.[24,31] The Raman in Figure 1c shows this region. It is evident that the wavenumber of TfO does not change much when the solvent is changed from formamide to NMF. However, a large shift to lower wavenumber occurs on using the aprotic solvents of DMF and DEF. This indicates that the Zn coordination changes significantly in protic and aprotic electrolytes and the side chain of the electrolytes also affects the interaction between the Zn salt and the solvent.

To understand the influence of change in the Zn speciation, the electrolytes were tested in a Zn symmetric cell. Figure 2 compares the galvanostatic performance of Zn deposition/stripping from different electrolytes at a current density of 1 mA cm^{-2}. Comparing the voltage time graphs in Figure 2, it is evident that the most stable Zn deposition/stripping takes place in formamide and NMF electrolytes (Figure 2a, Figure 2b).

Some stability is also achieved in 0.5 M $Zn(OTf)_2$ in DEF (Figure 2d). However, the Zn deposition/stripping stability is

Research Article
doi.org/10.1002/batt.202400140
Chemistry Europe
European Chemical Societies Publishing

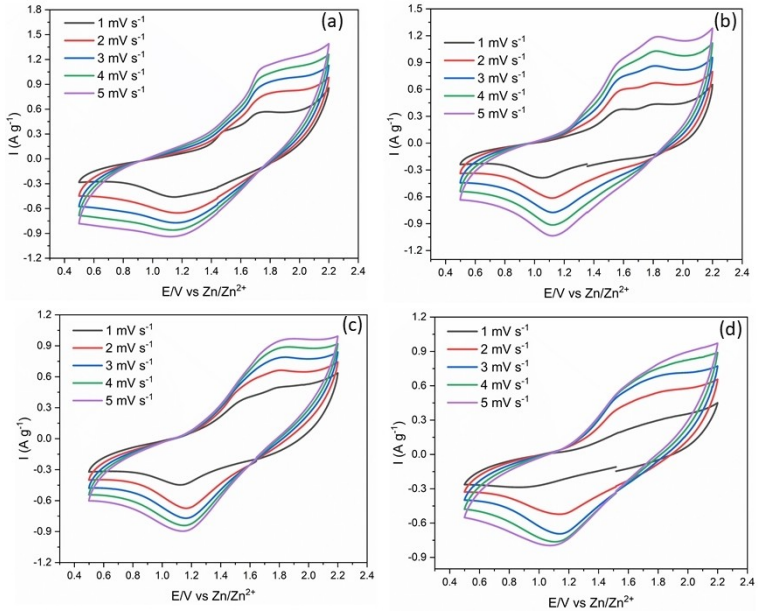

Figure 4. CV of Zn electrochemistry on MnO_2 in (a) 0.5 M $Zn(OTf)_2$ in Formamide (b) 0.5 M $Zn(OTf)_2$ in N-methyl Formamide (c) 0.5 M $Zn(OTf)_2$ in N,N dimethyl Formamide (d) 0.5 M $Zn(OTf)_2$ in N,N diethyl Formamide.

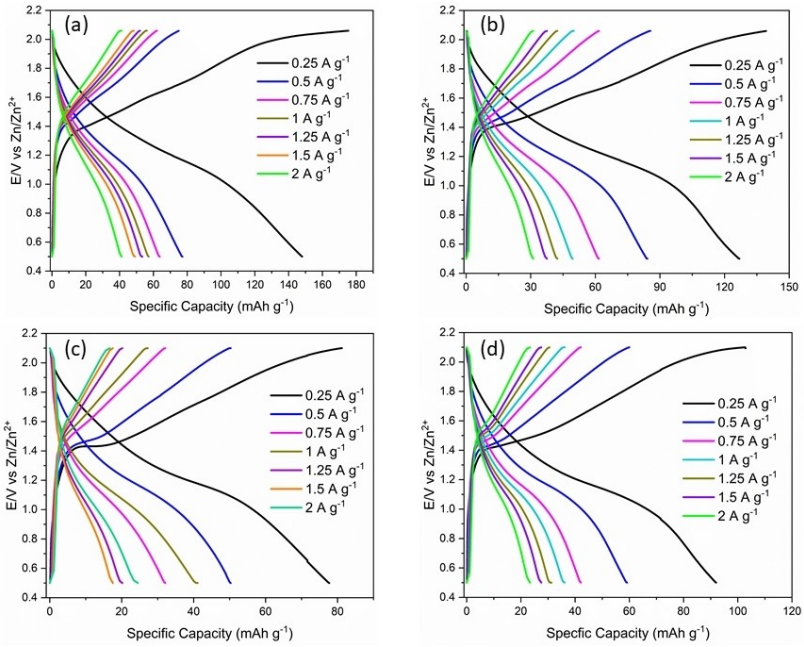

Figure 5. Charge discharge profile of Zn-MnO_2 at different current densities in (a) 0.5 M $Zn(OTf)_2$ in formamide (b) 0.5 M $Zn(OTf)_2$ in NMF (c) 0.5 M $Zn(OTf)_2$ in DMF (d) 0.5 M $Zn(OTf)_2$ in DEF, electrolytes.

worse in DMF electrolytes. Based on the Zn deposition/stripping experiments, it is evident that side chains affect the Zn electrochemistry significantly. Furthermore, comparing the protic electrolytes, the overpotential of Zn deposition is least for $Zn(OTf)_2$ in formamide.

To further access the Zn deposition/stripping phenomena, SEM and XRD were performed. Figure 3a–3d shows the morphology of Zn after deposition/stripping cycles. From the formamide electrolyte, the formation of the Zn nanoplate structure is evident. In comparison, the Zn morphology from NMF and DEF (Figure 3b and c) show a network-like structure whereas a porous structure is observed on using DMF (Figures 3d). Comparing the SEM, it is evident that the porous structure for aprotic electrolytes is much higher than the porous structure for protic electrolytes. The XRD of the Zn electrode after deposition/stripping is shown in Figure 3e. It is evident that based on the electrolyte used, the ratio of Zn(101)/Zn(002) changes significantly. For the case of formamide and DEF, this

Research Article
doi.org/10.1002/batt.202400140
Chemistry Europe
European Chemical Societies Publishing

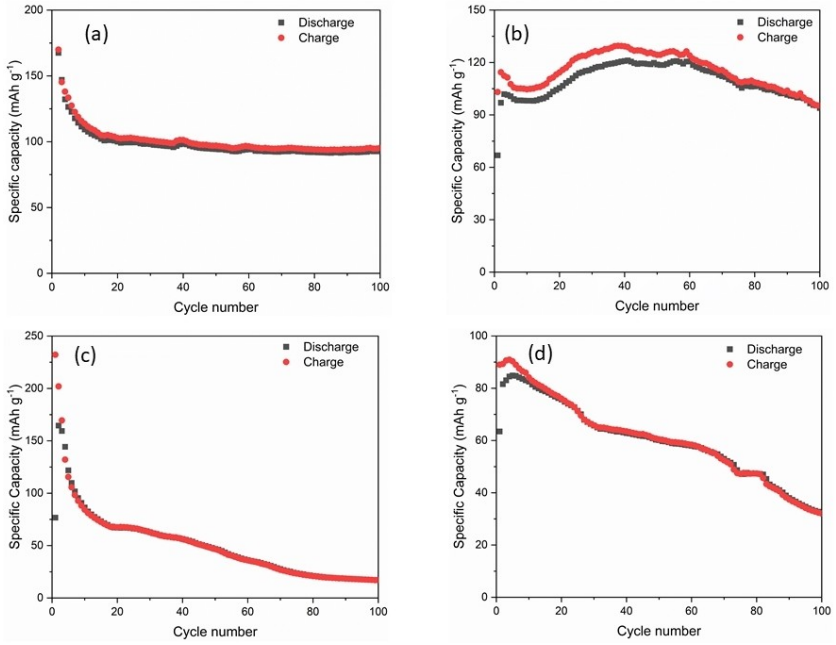

Figure 6. Cycling performance of Zn-MnO_2 at 0.25 A g^{-1} (a) 0.5 M $Zn(OTf)_2$ in formamide (b) 0.5 M $Zn(OTf)_2$ in NMF (c) 0.5 M $Zn(OTf)_2$ in DMF (d) 0.5 M $Zn(OTf)_2$ in DEF, electrolytes.

ratio is low (1.16) whereas for NMF (1.36) and DMF (1.2) the ratio is higher. It has been shown that Zn(100) and Zn(101) show high self-diffusion barrier whereas Zn(002) show high chemical stability as their surface energy is lower than that of (100) and (101) planes.[32] Therefore, an increase in Zn(002) plane appears to be a useful method to stabilise the Zn anode. Comparing the XRD in Figure 3e, it is evident that the peak intensity of Zn(002) is high for formamide and therefore shows a better Zn deposition/stripping cycle seen in Figure 2.

Next, we tested the electrolytes on an electrodeposited MnO_2 cathode. Figure 4 compares the Zn electrochemistry on MnO_2 from different electrolytes. In formamide electrolyte, at a lower scan rate (1 mV sec^{-1}, Figure 4a) two oxidation peaks at 1.5 and 1.7 V are observed and a single broad reduction wave peaking at 1.2 V is seen. With the increase in scan rate the two oxidation peaks merge to form a shoulder and a broad wave. These peaks can be ascribed to the Zn intercalation/deintercalation process in the MnO_2 matrix.[33]

On using NMF electrolyte, a similar feature is observed in Figure 4b. The oxidation peak occurs at 1.6 and 1.8 V and the reduction peak occurs at 1.15 V which can again be related to Zn intercalation/deintercalation process. However, compared to formamide with an increase in scan rate, the two oxidation peaks remain consistent. On using an aprotic electrolyte of N-dimethyl formamide, the CV (Figure 4c) again shows two oxidation peaks at 1.5 and 1.75 V and one reduction peak at 1.2 V whereas for N-diethyl formamide, a shoulder at 1.5 V and a peak at 1.8 V is observed in the oxidation scan (Figure 4d) and a reduction peak is observed at 1.15 V. Comparing the four CV curves in Figure 4, it is evident that the current density of using aprotic electrolytes is lower than protic electrolytes which could be due to higher viscosity and change in the Zn solvation structure in the electrolyte.

To understand the effect of the electrolyte on the capacity of the Zn-MnO_2 battery, galvanostatic charge-discharge was performed at different current densities. Figure 5 compares the charge-discharge behaviour at different current densities. The open circuit potential was found to be close to 1.5 V for formamide which decreased to close to 1.4 V on changing the electrolyte to NMF, NDMF, and NDEF.

The capacity obtained for formamide was 150 mAh g^{-1} at 0.25 A g^{-1} which decreased considerably to 80 mAh g^{-1} at 0.5 A g^{-1}, Figure 5a. In comparison, NMF showed a capacity of 130 mAh g^{-1} at 0.25 A g^{-1} which decreased to around 80 mAh g^{-1} at 0.5 A g^{-1}. On using the aprotic organic electrolytes, both DMF and DEF showed a capacity of 80 and 90 mAh g^{-1} at 0.25 A g^{-1}(figure 5c and 5d). Based on the results from Figure 5, it is evident that the battery capacity of protic organic solvents is much higher than the aprotic organic solvent. Furthermore, the side chain in formamide appears to decrease the battery capacity.

The cyclability of the battery was subsequently tested for the Zn/MnO_2 battery in different electrolytes at 0.25 A g^{-1}. Figure 6a shows the battery capacity and stability in formamide electrolyte when cycled between 0.5 and 2.1 V. An initial discharge capacity close to 160 mAh g^{-1} is observed which drops quickly to about 100 mAh g^{-1} and remains stable for 100 cycles. Repeated experiments showed that the drop in the capacity varied and an average capacity retention of 72% could be achieved. For the case of Zn containing NMP electrolyte, an initial discharge capacity of 105 mAh g^{-1} is achieved which increases to 110 mAh g^{-1} and then decreases to 93 mAh g^{-1} after 100 cycles (figure 6b). The change in the behaviour in Zn

storage can be ascribed to inhomogeneous deposition during charging as observed during Zn deposition/stripping process and from the Zn microstructure. For the case of aprotic electrolytes (Figure 6c and 6d), the stability of the Zn/MnO_2 battery decreases significantly. For the case of DMF, an initial discharge capacity of 170 $mAh\,g^{-1}$ is observed which decreases to less than 25 $mAh\,g^{-1}$ after 100 cycles whereas for DEF a decrease from 80 $mAh\,g^{-1}$ to less than 40 $mAh\,g^{-1}$ is observed. Thus, comparing the protic organic electrolytes to their aprotic counterpart, it is evident that protic electrolytes are better suited for the Zn/MnO_2 battery.

Conclusions

In this study, the influence of protic and aprotic electrolytes on $Zn\text{-}MnO_2$ battery was investigated. From spectroscopic analyses, it is evident that Zn solvation changes with a change in organic solvent, which affects the Zn deposition/stripping process significantly. It was observed that among all the electrolytes investigated, formamide showed the lowest Zn deposition overpotential and showed good cyclability. The electrochemistry of the Zn intercalation/deintercalation process in MnO_2 did not show a significant difference in all the electrolytes. However, the battery storage capacity depended on the electrolyte. Compared to aprotic organic electrolytes, the protic electrolytes not only showed a higher Zn storage capacity but also showed better stability.

Acknowledgements

This research was funded, in whole by EPSRC, EP/W015129/1.

Conflict of Interests

The authors declare no conflict of interest.

Data Availability Statement

The data that support the findings of this study are openly available in Brunel Figshare at https://doi.org/10.17633/rd.brunel.25093388.v1.

Keywords: Zn-ion batteries · Manganese dioxide · Organic electrolytes · Zn solvation · Formamide

[1] B. Dunn, H. Kamath, J.-M. Tarascon, *Science* **2011**, *334*, 928–935.
[2] Y. Zeng, Z. Lai, Y. Han, H. Zhang, S. Xie, X. Lu, *Adv. Mater.* **2018**, *30*, 1802396.
[3] N. Nitta, F. Wu, J. T. Lee, G. Yushin, *Mater. Today* **2015**, *18*, 252–264.
[4] C. M. Costa, J. C. Barbosa, R. Goncalves, H. Castro, F. J. Del Campo, S. Lanceros-Mendez, *Energy Storage Mater.* **2021**, *37*, 433–465.
[5] J.-M. Tarascon, M. Armand, *Nature* **2001**, *414*, 359–367.
[6] K. Kubota, M. Dahbi, T. Hosaka, S. Kumakura, S. Komaba, *The chemical record* **2018**, *18*, 459–479.
[7] L. Peng, Y. Zhu, D. Chen, R. S. Ruoff, G. Yu, *Adv. Energy Mater.* **2016**, *6*, 1600025.
[8] J. Chen, D. H. C. Chua, P. S. Lee, *Small Methods* **2020**, *4*, 1900648.
[9] B. Tang, L. Shan, S. Liang, J. Zhou, *Energy Environ. Sci.* **2019**, *12*, 3288–3304.
[10] G. Fang, J. Zhou, A. Pan, S. Liang, *ACS Energy Lett.* **2018**, *3*, 2480–2501.
[11] L. E. Blanc, D. Kundu, L. F. Nazar, *Joule* **2020**, *4*, 771–799.
[12] S. Zhang, N. Yu, S. Zeng, S. Zhou, et al., *J. Mater.Chem A* **2018**, *6*, 12237–12243.
[13] C. Xu, B. Li, H. Du, F. Kang, *Angew. Chem. Int. Ed.* **2012**, *51*, 933–935.
[14] W. Sun, F. Wang, S. Hou, C. Yang, et al., *J. Am. Chem. Soc.* **2017**, *139*, 9775–9778.
[15] X. Gao, H. Wu, W. Li, Y. Tian, et al., *Small* **2020**, *16*, 1905842.
[16] M. Han, L. Qin, Z. Liu, L. Zhang, et al., *Mater. Today. Energy.* **2021**, *20*, 100626.
[17] M. S. Chae, J. W. Heo, H. H. Kwak, H. Lee, et al., *J. Power Sources* **2017**, *337*, 204–211.
[18] Y. Zuo, K. Wang, P. Pei, M. Wei, et al., *Mater. Today. Energy.* **2021**, *20*, 100692.
[19] K. E. K. Sun, T. K. A. Hoang, T. N. L. Doan, Y. Yu, et al., *ACS Appl. Mater. Interfaces* **2017**, *9*, 9681–9687.
[20] Y. Lv, Y. Xiao, L. Ma, C. Zhi, S. Chen, *Adv. Mater.* **2022**, *34*, 2106409.
[21] D. Kundu, S. H. Vajargah, L. Wan, B. Adams, D. Prendergast, L. F. Nazar, *Energy Environ. Sci.* **2018**, *11*, 881–892.
[22] Z. Liu, T. Cui, G. Pulletikurthi, A. Lahiri, T. Carstens, M. Olschewski, F. Endres, *Angew. Chem. Int. Ed.* **2016**, *55*, 2889–2893.
[23] Z. Liu, G. Li, T. Cui, A. Lahiri, A. Borodin, F. Endres, *Phys. Chem. Chem. Phys.* **2017**, *19*, 25989–25995.
[24] T. Cui, A. Lahiri, T. Carstens, N. Borisenko, G. Pulletikurthi, C. Kuhl, F. Endres, *J. Phys. Chem. C* **2016**, *120*, 9341–9349.
[25] A. Lahiri, L. Yang, G. Li, F. Endres, *ACS Appl. Mater. Interfaces* **2019**, *11*, 45098–45701.
[26] C. Pan, R. G. Nuzzo, A. A. Gewirth, *Chem. Mater.* **2017**, *29*, 9351–9359.
[27] S.-D. Han, S. Kim, D. Li, V. Petkov, et al., *Chem. Mater.* **2017**, *29*, 4874–4884.
[28] W. Kai-ian, M. T. Nguyen, T. Yonezawa, R. Pornprasertsuk, J. Qin, S. Siwamogsatham, S. Kheawhom, *Materials. Today. Energy.* **2021**, *21*, 100738.
[29] J. W. Essex, W. L. Jorgensen, *J. Phys. Chem.* **1995**, *99*, 17956–17962.
[30] J. Richardi, H. Krienke, P. H. Fries, *Chem. Phys. Lett.* **1997**, *273*, 115–121.
[31] A. Lahiri, S. Guan, A. Chutia, *ACS Applied Energy. Mater.* **2023**, *6*, 11874–11881.
[32] S. Wu, Z. Hu, P. He, L. Ren, J. Huang, J. Luo, *eScience* **2023**, *3*, 100120.
[33] S.-D. Han, S. Kim, D. Li, V. Petkov, H. D. Yoo, P. J. Phillips, H. Wang, J. J. Kim, K. L. More, B. Key, R. F. Klie, J. Carbana, V. R. Stamenkovic, T. T. Fister, N. M. Markovic, A. K. Burrell, S. Tepavcevic, J. T. Vaughey, *Chem. Mater.* **2017**, *29*, 4874–4884.

Manuscript received: March 2, 2024
Revised manuscript received: April 9, 2024
Accepted manuscript online: April 24, 2024
Version of record online: May 28, 2024